Journal of Alloys and Compounds 527 (2012) 197–203

Contents lists available at SciVerse ScienceDirect

Journal of Alloys and Compounds

journal homepage: www.elsevier.com/locate/jallcom

Density functional study of structural and electronic properties of Al_nAs $(1 \leq n \leq 15)$ clusters

Ling Guo

School of Chemistry and Material Science, Shanxi Normal University, Linfen 041004, China

ARTICLE INFO

Article history:
Received 13 December 2011
Received in revised form 29 February 2012
Accepted 3 March 2012
Available online xxx

Keywords:
Al_nAs cluster
DFT theory
Stability

ABSTRACT

Energetically low-lying equilibrium geometric structures of Al_nAs (n = 1–15) clusters obtained by an all-electron linear combination of atomic orbital approach, within spin-polarized density functional theory, are reported. The binding energy, dissociation energy, and stability of these clusters are studied with the three-parameter hybrid generalized gradient approximation (GGA) due to Becke–Lee–Yang–Parr (B3LYP). Ionization potentials, electron affinities, hardness, and static dipole polarizabilities are calculated for the ground-state structures within the same method. The growth pattern for Al_nAs (n = 1–15) clusters is As-substituted the surface atom of Al_{n+1} clusters and it keeps the similar frameworks of the most stable Al_{n+1} clusters except for Al_nAs (n = 7, 8, and 15) clusters. The odd–even oscillations in the dissociation energy, the second differences in energy, the HOMO–LUMO gaps, the electron affinity, and the hardness are more pronounced. The stability analysis based on the energies clearly shows the clusters with an even number of valence electrons are more stable than clusters with odd number of valence electrons.

1. Introduction

Small clusters composed of aluminum atom have been the subjects of intensive studies for the last two decades. A large number of studies of aluminum clusters, both theoretical and experimental have been reported (see, for example, the reviews in Refs. [1–3]). One of the main motivations behind these studies is to understand the evolution of physical properties with the size of the cluster. Many properties of aluminum clusters can be understood using the spherical jellium model (SJM) [4], in which the ions are smeared out in a uniformly charged sphere leading to electronic shell closures for clusters containing a 'magic' number 2, 8, 20, 40, 58, 92, 138, ... of valence electrons. These findings are subsequently confirmed by first-principles theoretical calculations in which the ions are represented by pseudopotentials [5]. The question we address here is the effect of doping by a single impurity on the electronic structure and geometry of these clusters. In bulk materials, a small percentage of impurity is known to affect the properties significantly. In clusters, the impurity effect should be even more pronounced and influenced by the finite size of the system. Under vacuum condition and using magnetron reactive sputtering technique, the sputtering technique, the sputtered Al atoms can react with As to form a new-type AlAs nanofilm, and some Al_nAs precursor intermediates have been experimentally already observed [6]. This experimental work triggered an interest in simulations of As doped aluminum clusters. Ab initio calculations on properties of Al_xAs_y clusters have been carried out by several groups [7–13]. Andreoni [7] calculated the structures, stability, and melting of $(AlAs)_n$ (n = 2–5) using the Car-parrinello method. Quek et al. [8] reported tight binding molecular dynamics studies of the structures of Al_mAs_n ($m + n \leq 13$). Tozzini et al. [9] presented extensive theoretical calculations of the geometric and electronic properties of neutral and ionized AlAs fullerene-like clusters of the type Al_xAs_{x+4} with a number of atoms up to 52, on the basis of density functional theory. Costales et al. [10] used density functional theory (DFT) to explore structural and vibration properties for $(AlAs)_n$ clusters up to 6 atoms, finding the same behavior as in the aluminum nitride clusters. Archibong and St-Amant [11] calculated the low-lying electronic states of Al_3As, $AlAs_3$, and the corresponding anions at the B3LYP and CCSD(T) levels of theory using the 6-311+G(2df) one-particle basis set. The adiabatic electron affinities, electron detachment energies and harmonic vibration frequencies of both the anions and the neutral molecules are presented and discussed. Feng et al. [12] reported a MRSDCI study of the ground and several energetically low-lying excited states of Al_2As_3, Al_3As_2, and their ions. Recently, Zhu [13] studied the spectroscopic properties for Al_2As, $AlAs_2$, and their ions using density functional theory (DFT: B3LYP) and complete active space multiconfiguration self-consistent field (CASSCF) calculations.

To provide further insight on Al_nAs clusters, I have carried out a detailed systematic study of the equilibrium structure and various electronic-structure related properties of these clusters, employing the hybrid generalized gradient approximation (GGA) for the exchange-correlation potential. I investigate the relative

E-mail address: gl-guoling@163.com

0925-8388/$ – see front matter © 2012 Elsevier B.V. All rights reserved.
doi:10.1016/j.jallcom.2012.03.013

Table 1
Calculated bond lengths, vibrational frequencies, and vertical electronic detachment, experimental results, and previous theoretical study.

	As_2			Al_2	
	Our work	Theoretical	Experimental	Our work	Experimental[c]
Bond length (Å)	2.11	2.13[a]	2.10[b]	2.56	2.56
w (cm^{-1})	431	422	430	323.10	350.01
VDE (eV)				1.43	1.55

[a] Ref. [22].
[b] Ref. [23].
[c] Ref. [24].

ordering of these structures with the As impurity occupying the outside and other position. Here, the evolution of the ionization potential, electron affinity, HOMO–LUMO gap, hardness, polarizability, dissociation energy, and binding energy for Al_nAs clusters up to $n = 15$ have been studied. These physical quantities are compared with their counterparts calculated at the same level (all-electron B3LYP/6-311+G*) for pure aluminum clusters.

In the following section, the computational methodology has been briefly outlined. In Section 2 the results are presented and discussed, and some conclusions are given in Section 3.

2. Methodology and computational details

The geometry optimization and electronic-structure calculation is carried out using a molecular-orbital approach within the framework of spin-polarized density functional theory [14,15]. An all-electron 6-311+G* basis set is employed [16]. KS exchange along with the Vosko–Wilk–Nusair [17] parametrization of homogeneous electron gas data due to Ceperley and Alder [18] have been employed. In this case, Becke's three parameter functional (B3LYP) [19] has been used, which use part of the Hartree–Fock exchange (but calculated with KS orbitals) and Becke's exchange functional [20] in conjunction with the Lee–Yang–Parr [21] functional for correlation. Frequency analysis is performed at the B3LYP/6-31G* level to check whether the optimized structures are transition states or true minima on the potential energy surfaces of corresponding clusters. And all ground-state structures are actually equilibrium states without imaginary frequencies. The configuration is regarded as optimized when the maximum force, the root mean square (rms) force, the maximum displacement of atoms, and the rms displacement of atoms have magnitudes less than 0.0045, 0.0003, 0.0018, and 0.0012 a.u., respectively. The calculations are carried out for spin multiplicities of $2S + 1 = 1$ and $2S + 1 = 2$ for clusters with even and odd numbers of electrons, respectively. All calculations are carried out using GAUSSIAN 03 [19] suite of programs.

The accuracy of the current computational scheme has been tested by the calculation on the As_2 and Al_2 dimer. The results are summarized in Table 1. For As_2, we obtain a bond length (2.11 Å) that fits well with the theoretical values of 2.13 Å by the GGA using BLYP function [22]. And the optimized bond length and vibration frequency of 2.11 Å and 431 cm^{-1} compare favorably with the experimental value of 2.10 Å and 430 cm^{-1} [23]. Additionally, the bond length (2.56 Å), vibration frequency (323.10 cm^{-1}), and the vertical electron detachment energy (1.43 eV) of Al_2 are obtained, which are in agreement with the experimental values [24] of 2.56 Å, 350.01 cm^{-1}, and 1.55 eV, respectively. This indicates that our approach provides an efficient way to study small Al_nAs clusters.

3. Results and discussion

3.1. Atomic structures

The ground state geometries of Al_nAs ($n = 1$–15) clusters, and some energetically low-lying metastable isomer are shown in Fig. 1. For proper comparison we have also shown the ground state geometries of pure Al_n ($n = 2$–16) clusters. The symmetries, the spin multiplicities, and the electronic states of the most stable and energetically low-lying Al_nAs ($n = 1$–15) clusters are summarized in Table 2. For the AlAs dimer with $C_{\infty v}$ symmetry, the optimized results indicate that the triplet spin state is lower in total energy than the singlet and quintet isomers by 0.80 eV and 1.80 eV, respectively. Therefore, the triplet AlAs dimer (1a in Fig. 1) with a bond length of 2.328 Å is the most stable structure.

The lowest-energy structure of Al_3 is an equilateral triangle structure with D_{3h} symmetry (2a_0 in Fig. 1). In the B3LYP scheme, the lowest-energy structure for Al_2As is an isosceles triangle with As at the apex (2a in Fig. 1). The Al—As bond length of the ground state Al_2As molecule are 2.35 Å using the B3LYP schemes, which is similar with the value 2.39 Å reported by Zhu [25] obtained from CASSCF calculation.

Al_4 is a square with D_{4h} symmetry (3a_0 in Fig. 1). Two energetically low-lying structures are found for Al_3As in the B3LYP scheme. The most stable one (3a in Fig. 1) consists of a central As atom surrounded by three Al atoms in form of an equilateral triangle. The other energetically degenerate structure (3b in Fig. 1) is a distorted rhombus and is above the most stable by 0.10 eV. It may be noted that the order of isomers is reversed in the LSDA, with the distorted

Table 2
The symmetries (sym), the spin multiplicities (multi), and the energies (E_t, hartree/particle) of the most stable and energetically low-lying Al_nAs ($n = 1$–15) clusters (the isomers are labeled as na and nb: the na corresponds to the lowest-energy isomer).

Cluster	Isomer	Sym	Multi	E_t
AlAs	1a	$C_{\infty v}$	3	−2478.2758
Al_2As	2a	C_{2v}	2	−2720.7648
Al_3As	3a	C_{2v}	1	−2963.2500
	3b	C_{2v}	1	−2963.2465
Al_4As	4a	C_{2v}	2	−3205.7014
	4b	C_s	2	−3205.6746
Al_5As	5a	C_s	3	−3448.1717
	5b	C_s	1	−3448.1628
Al_6As	6a	C_1	2	−3690.6231
	6b	C_{2v}	2	−3690.6165
Al_7As	7a	C_1	1	−3933.0939
	7b	C_1	1	−3933.0840
Al_8As	8a	C_1	2	−4175.5564
	8b	C_s	2	−4175.5556
Al_9As	9a	C_1	1	−4418.0295
	9b	C_1	1	−4418.0221
$Al_{10}As$	10a	C_1	2	−4660.4901
	10b	C_1	2	−4660.4762
$Al_{11}As$	11a	C_1	1	−4902.9771
	11b	C_1	1	−4902.9507
$Al_{12}As$	12a	C_1	2	−5145.4377
	12b	C_1	2	−5145.4315
$Al_{13}As$	13a	C_1	1	−5387.9204
	13b	C_1	1	−5387.8904
$Al_{14}As$	14a	C_1	2	−5630.4124
	14b	C_1	2	−5630.3462
$Al_{15}As$	15a	C_1	1	−5872.9087
	15b	C_1	1	−5872.8668

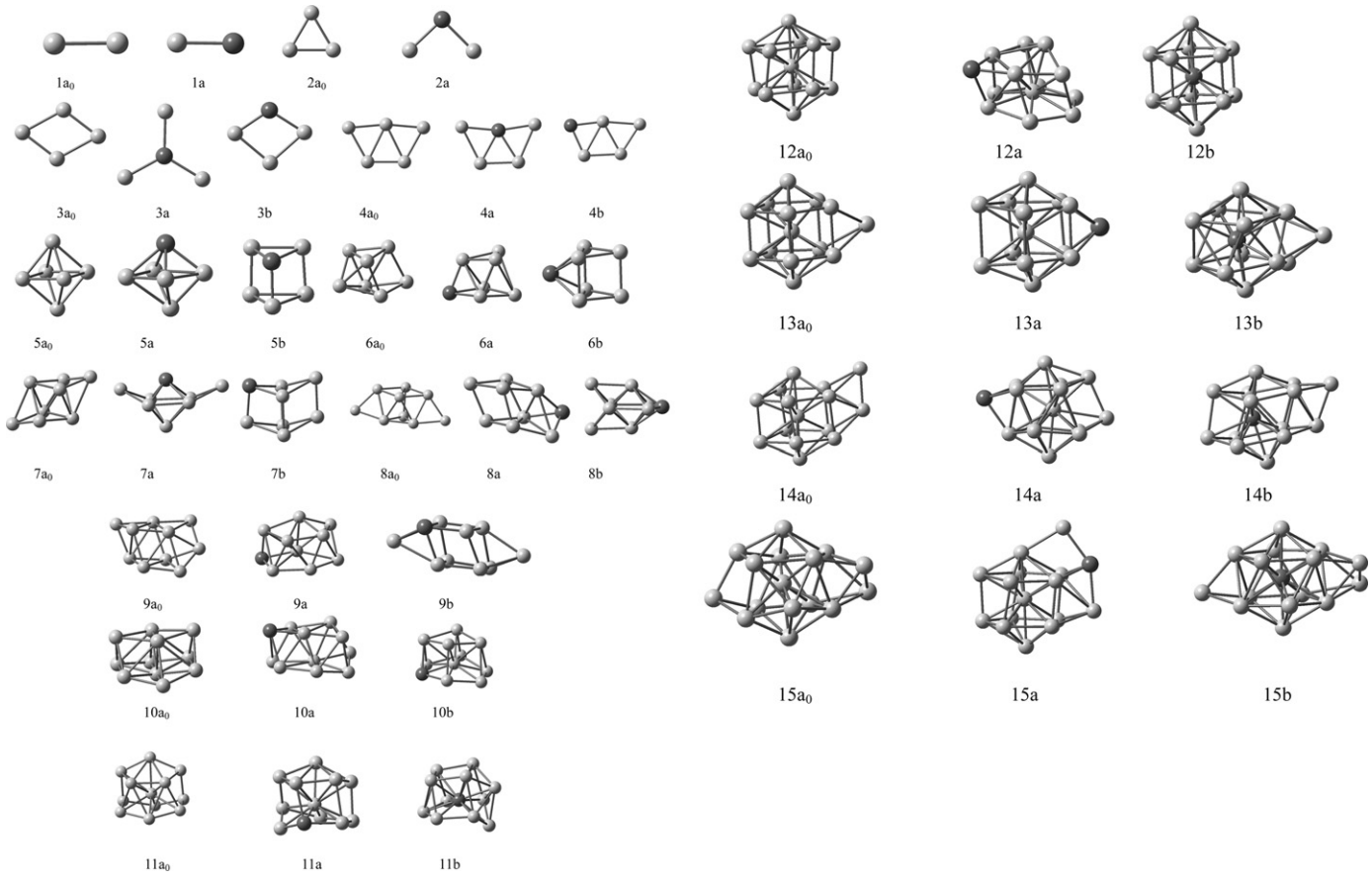

Fig. 1. Geometries of Al_nAs structures.

rhombus being the most stable one. In LSDA, the structure (3a in Fig. 1) is 0.28 eV higher in energy than 3b.

For Al_5, the most stable structure is a pentagon structure with C_s symmetry ($4a_0$ in Fig. 1). In the case of Al_4As, two energetically low-lying nearly degenerate planar structures are found. For Al_4As, the structure with C_{2v} symmetry (4a in Fig. 1) is similar to the Al_5 configuration, where the impurity As atom is at its vertex position. The energetically low-lying isomer (4b in Fig. 1) with a higher energy (0.73 eV) is also a pentagon configuration.

As for Al_6, the lowest-energy structure is a prism structure with C_{2v} ($^3B_1$) symmetry ($5a_0$ in Fig. 1). For Al_5As, As occupies apical positions in both the nearly degenerate octahedron (5a in Fig. 1) and the prism structures (5b in Fig. 1). The As impurity in the ground state structure (5a in Fig. 1) can be look upon as the substitutional impurity in the ground state Al_6 cluster.

In the case of $n = 7$, the pure Al_7 ($6a_0$ in Fig. 1) adopted the distorted capped trigonal prism with C_1 symmetry. The As impurity capping the lowest-energy structure of Al_6 forms the ground state of Al_6As (6a in Fig. 1). A face-capped triangle prism with the As atom being the capping atom (6b in Fig. 1) is higher in energy than the lowest-energy structure by 0.19 eV.

The lowest-energy configuration of Al_8 ($7a_0$ in Fig. 1) is the rhombic prism with D_{2h} symmetry. Substituting one Al atom of cubelike Al_8 cluster with As impurity makes up of the energetically low-lying structure of Al_7As (7b in Fig. 1). This geometry of Al_7As is in competition with the ground-state structure (7a in Fig. 1). The energy difference between the two structures is merely 0.27 eV.

The lowest-energy structure of Al_9 ($8a_0$ in Fig. 1) develops pentagonal arrangements of atoms. A As atom capped distorted rhombic prism of Al_8 clusters yields the lowest-energy structure for the Al_8As cluster (8a in Fig. 1). The energetically low-lying geometry (8b in Fig. 1) of Al_8As is the result of the addition of the two Al atoms and As impurity to the energetically low-lying geometry of Al_6 cluster, which caps the different sides. The structure (8b in Fig. 1) is higher by 0.02 eV.

Two pentagons overlapped can form the lowest-energy structure of Al_{10} ($9a_0$ in Fig. 1). For Al_9As cluster, the ground state geometry (9a in Fig. 1) is the As atom substitute one capping Al atom of Al_{10} with C_1 symmetry. The structure of isomer (9b in Fig. 1) is above the lowest-energy structure by 0.20 eV, which is bicapped hexagonal bipyramid with C_1 symmetry.

The most stable structure of Al_{11} develops pentagonal arrangements of atoms. In these aluminum clusters with $n > 10$, an interior atom with bulklike coordination emerges. The ground state (10a in Fig. 1) and the energetically low-lying geometries of $Al_{10}As$ (10b in Fig. 1) clusters can also be seen as substitutional the different position structures of Al_{11} ($10a_0$ in Fig. 1). The energy different is 0.42 eV.

Al_{12} with C_1 symmetry ($11a_0$ in Fig. 1) can be obtained by continuing to develop pentagonal arrangements of atoms. When the As atom is adsorbed on the surface of Al_{12}, this forms the ground state geometry (11a in Fig. 1) with C_1 symmetry. By substituting one As atom for one Al atom in the center of the Al_{12}, we can obtain the energetically low-lying geometry of $Al_{11}As$ (11b in Fig. 1) with C_1 symmetry by 0.73 eV.

For the case of Al_{13}, the lowest energy structure ($12a_0$ in Fig. 1) is a distorted decahedron with C_s symmetry. The top surface Al atom substituting by the impurity As atom can get the most stable structure of $Al_{12}As$ with C_1 symmetry (12a in Fig. 1). The ground state structure of $Al_{12}As$ is not in agreement with the ground state geometries of $Y_{12}Al$, $Ti_{12}Al$, and $Al_{12}N$ clusters [26–28]. The energetically low-lying structure (12b in Fig. 1), 0.17 eV higher than a,

with C_1 symmetry is a decahedron structure with the As atom in the cage center, which is similar to Al_{13} ($12a_0$ in Fig. 1).

Capped one Al atom on decahedron with C_1 symmetry is obtained for pure Al_{14} ($13a_0$ in Fig. 1). The most stable $Al_{13}As$ (13a in Fig. 1) with C_1 symmetry is capped one Al atom on the Al_{13} geometry. Another isomer (13b in Fig. 1) is the As atom substituting the central Al atom in the Al_{14} cluster, which is 0.80 eV higher in energy.

For Al_{15} ($14a_0$ in Fig. 1), the geometry results by capping one of the square faces of the Al_{13} by two atoms. This results in a slight distortion of the Al_{13} with C_1 symmetry. For $Al_{14}As$ cluster, the ground state geometry (14a in Fig. 1) with C_1 symmetry is the As atom capping the surface of the Al_{15} cluster. The energetically low-lying isomer (14b in Fig. 1) is the As atom that falls into the center of Al_{15} with C_1 symmetry. Their energy difference is 1.80 eV.

The lowest-energy structure of Al_{16} ($15a_0$ in Fig. 1) is formed by capping one of the square faces of Al_{15}. The ground state geometry (15a in Fig. 1) of $Al_{15}As$ cluster with C_1 symmetry can be seen as adding Al atom in Al_{15} cluster and As impurity replacing the outside Al atom in the Al_{15} cluster. Another isomer (15b in Fig. 1) is the As atom replacing the central Al atom in the Al_{16} clusters, which is 1.14 eV higher in energy.

In summary, the growth pattern for most different sized Al_nAs (n = 1–6, 9–14) clusters is As atom substituting the surface atom of the Al_{n+1} clusters. And for Al_8As and $Al_{15}As$ clusters, the As impurity occupies a peripheral position of Al_8 and Al_{15} clusters, respectively. The Al_7As does not conform to the above rule.

3.2. Stabilities and electronic properties

We now discuss the relative stability of these clusters by computing the energetic that is indicative of the stability. We compute the atomization or binding energy (E_b) per atom, the dissociation energy (ΔE), and the second differences of energy ($\Delta_2 E$) as, respectively,

$$E_b[Al_nAs] = \frac{nE[Al] + E[As] - [Al_nAs]}{n+1}, \quad (1)$$

$$\Delta E[Al_nAs] = E[Al_nAs] - E[Al_{n-1}As] - E[Al], \quad (2)$$

$$\Delta_2 E[Al_nAs] = E[Al_{n+1}As] + E[Al_{n-1}As] - 2E[Al_nAs] \quad (3)$$

The E_b of the Al_nAs clusters (shown in Fig. 2) is calculated using Eq. (1), where E(Al), E(As), and $E(Al_nAs)$ represent the energies of an Al atom, an As atom, and the total energy of the Al_nAs cluster, respectively. For comparison, we also plot the E_b of the host Al_n cluster, $E_b[Al_n] = (nE[Al] - E[Al_n])/n$, in Fig. 2.

In general the E_b increases sharply for very small clusters and then follows a plateau as the cluster size grows. Small humps or

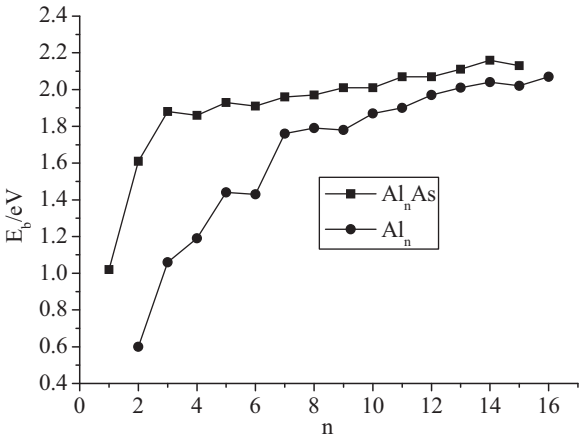

Fig. 2. The binding energy per atom of Al_nAs and Al_n clusters.

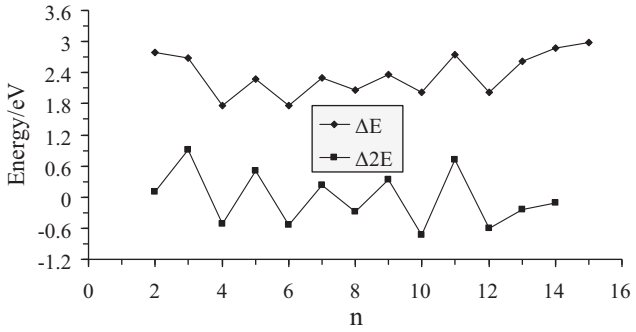

Fig. 3. The second-order energy difference $\Delta_2 E$ and the dissociation energy ΔE of the Al_nAs clusters.

dips for the specific size of clusters signify their relative stabilities. As seen in this figure, the average binding energies of the Al_nAs clusters are higher than those of the pure Al_n clusters. It indicates that the doped As atom in the Al_n clusters contributes to strengthen the stabilities of the aluminum framework. For Al_nAs, the E_b evolves monotonically with total number of atoms in the cluster. Especially, for n = 1–5, the E_b increases rapidly from 1.02 eV for AlAs to 1.93 eV for Al_5As which corresponds to the structure transition from two to three dimension. The E_b increases gradually in the range n = 6–15, in which the rate of increase becomes weak (only from 1.93 to 2.13 eV). In addition, the comparison of aluminum with the E_b curve for Al_nAs clusters shows that the small clusters of Al_nAs are strongly bound. As the cluster grows in size, the difference between the E_b curves of Al_nAs clusters and pure aluminum clusters stead diminishes, indicating that the bonding in doped clusters is essentially similar to that in pure clusters.

In cluster physics, the dissociation energy (ΔE) and the second-order energy differences ($\Delta_2 E$) are sensitive quantities that reflect the relative stability of the investigated clusters. The ΔE shows the energy that one atom is separated from the host clusters. The $\Delta_2 E$ is often compared directly with the relative abundances determined in mass spectroscopy experiments. They are defined as Eqs. (2) and (3). Where $E(Al_nAs)$, $E(Al_{n+1}As)$, $E(Al_{n-1}As)$, and E(Al) represent the total energies of the most stable Al_nAs, $Al_{n+1}As$, and $Al_{n-1}As$ clusters and an Al atom, respectively. As shown in Fig. 3, the curve shows odd–even oscillations with a peak for clusters with an even number of electrons, and particularly prominent maxima of $\Delta_2 E$ are found at n = 3, 5, 7, 9, 11, indicating higher stability than their neighboring clusters. It is observed that, for the Al_nAs cluster, the ΔE of Al_3As (2.69 eV), Al_5As (2.28 eV), Al_7As (2.30 eV), Al_9As (2.36 eV), $Al_{11}As$ (2.74 eV), $Al_{13}As$ (2.62 eV) and $Al_{15}As$ (2.99 eV) clusters are higher than their neighboring clusters.

We have also calculated the adsorption energy of As, i.e., the energy released upon adsorption of As by a pure aluminum cluster, according to

$$E_{ad} = E[Al_nAs] - E[Al_n] - E[As] \quad (4)$$

The calculated values of E_{ad} for the clusters up to $Al_{15}As$ ranges between 2.05 and 4.75 eV (Table 3). The minimum value (2.05 eV) occurs for AlAs, while it takes the maximum value (4.75 eV) for Al_6As.

The HOMO–LUMO gap (highest occupied-lowest unoccupied molecular orbital gap) is a useful quantity for examining the stability of clusters. It is found that systems with larger HOMO–LUMO gaps are, in general, less reactive. In the case of an odd-electron system, we calculate the HOMO–LUMO gap as the smallest spin-up–spin-down gap. The HOMO–LUMO gaps as thus calculated are presented in Fig. 4. For Al_nAs clusters, local peaks are found at n = 3, 5, 9, 11, 13, implying the chemical stability of these clusters is stronger than that of their neighboring clusters. The magic clusters

Table 3
Adsorption energies (in eV) (see text for full details) calculated within B3LYP with (6-311+G*) basis set.

n	1	2	3	4	5	6	7	8	9	10	11	12	13	14	15
E_{ad}	2.05	4.24	4.34	4.55	4.40	4.75	3.30	3.42	4.01	3.40	3.88	3.24	3.36	3.75	3.74

mostly have a very large HOMO–LUMO gap for the metal clusters. And I do find a strong correlation between the HOMO–LUMO gap and the energetic stability of the Al_nAs clusters except for Al_7As. We note that the HOMO–LUMO gaps of Al_nAs present a similar oscillating behavior as observed for the dissociation energy and the second difference. Clusters with an even number of electrons have a larger HOMO–LUMO energy gap and therefore are expected to be less reactive than clusters with an odd number of electrons. The stability exhibited by even number of electrons clusters is due to their closed-shell configurations that always come along with an extra stability. It is important to mention that this result is agreement with the electronic shell jellium model, where filled-shells cluster with 2, 8, 18, 20, 40, 58, 92, . . . valence electrons have increased stability, the mass spectra of cluster distribution shows pronounced intensity in clusters with these number of atoms, the so-called magic numbers.

Experimentally, the electronic structure is probed via measurements of ionization potentials, electron affinities, polarizabilities, etc. Therefore, we also study these quantities to understand their evolution with size. These quantities are determined within B3LYP for the lowest-energy structures obtained within the same scheme.

The vertical ionization potential (VIP) is calculated as the self-consistent energy difference between the cluster and its positive ion with the same geometry. The VIP is plotted in Fig. 5 as a function of cluster size. The corresponding data are given in Table 4. In general, the VIP decreases as the cluster size increases. The peaks occurring at Al_nAs (n = 1, 2, 5, 8, 9) are prominent, with large drops for the following clusters. Also shown in Fig. 5 are the VIPs of pure aluminum clusters. These have also been calculated at the B3LYP/6-311+G* level of theory, with structures optimized at the same level of theory. The comparison of the two curves shows that odd–even oscillations are not observed in both pure Al clusters and Al_nAs clusters in the whole range. It is also interesting to note that replacing one Al in Al_n cluster with As, to give $Al_{n-1}As$, results in the approximate values of VIPs for most clusters except for Al_nAs (n = 1–3 and 6), which have lager VIPs than the corresponding Al_n clusters.

We have also calculated vertical electron affinities (VEA) for these clusters (see Fig. 6 and Table 4) by assuming the geometry for the charged cluster to be the same as for the neutral one. The VEA exhibits an odd–even pattern. This is a consequence of the electron pairing effect. In the case of clusters with an even number of valence electrons, the extra electron has to go into the next orbital, which costs energy, resulting in a lower value of VEA. A comparison of the VEAs of Al_nAs clusters and pure aluminum clusters

Table 4
Vertical ionization potential (VIP) and vertical electron affinities (VEA) of Al_nAs (n = 1–15) clusters at B3LYP/6-311+g* level.

Cluster	VIP (eV)	VEA (eV)
AlAs	7.84	2.00
Al_2As	7.84	2.39
Al_3As	7.04	0.79
Al_4As	6.31	1.83
Al_5As	6.66	1.66
Al_6As	6.34	1.91
Al_7As	6.10	1.78
Al_8As	6.49	2.22
Al_9As	6.52	1.99
$Al_{10}As$	6.21	2.40
$Al_{11}As$	6.30	1.81
$Al_{12}As$	6.31	2.64
$Al_{13}As$	6.35	1.35
$Al_{14}As$	5.87	2.44
$Al_{15}As$	6.02	2.14

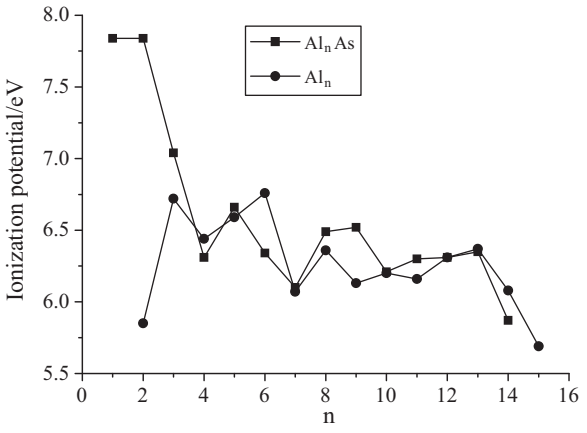

Fig. 5. Ionization potential for Al_nAs and Al_n clusters.

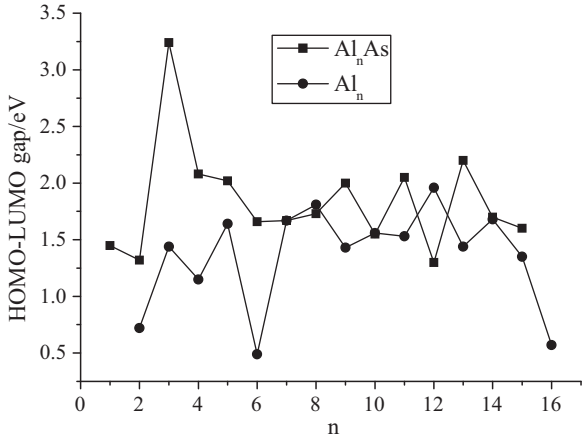

Fig. 4. The HOMO–LUMO gap of the Al_nAs and Al_n clusters.

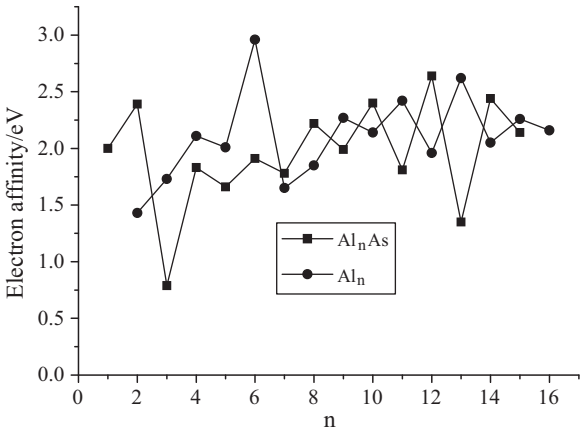

Fig. 6. Electron affinity for Al_nAs and Al_n clusters.

Table 5
Static mean polarizadbility $\langle\alpha\rangle$ and mean polarizability per atom $(\langle\alpha\rangle/n+1)$ of Al_nAs clusters calculated within the B3LYP with (6-311+G*) basis set. All values are in a.u.

System	α_{xx}	α_{yy}	α_{zz}	$\langle\alpha\rangle$	$\langle\alpha\rangle/n+1$
AlAs	128.6	41.9	104.2	91.6	45.8
Al_2As	72.0	270.9	101.1	148.0	49.3
Al_3As	224.7	224.7	105.7	185.0	46.3
Al_4As	122.0	331.7	225.3	226.3	45.3
Al_5As	195.9	256.6	269.1	240.5	40.1
Al_6As	313.7	276.4	265.8	285.3	40.8
Al_7As	526.7	289.8	243.6	353.4	44.2
Al_8As	475.3	337.5	299.3	370.7	41.2
Al_9As	489.5	361.1	380.2	410.3	41.0
$Al_{10}As$	534.6	417.5	381.7	444.6	40.4
$Al_{11}As$	460.9	514.8	451.7	475.8	39.7
$Al_{12}As$	540.5	544.7	426.9	504.0	38.8
$Al_{13}As$	558.9	533.8	506.2	533.0	38.1
$Al_{14}As$	623.7	520.1	519.9	554.6	37.1
$Al_{15}As$	685.2	593.8	500.6	593.2	37.0

again shows that the most Al_n and $Al_{n-1}As$ have the approximate values of VEAs. This observation is consistent with the observations from VIPs.

Another useful quantity is the chemical hardness [29], which can be approximated as

$$\eta \approx \frac{1}{2(I-A)} \approx \frac{1}{2(\varepsilon_L - \varepsilon_H)}, \quad (5)$$

where A and I are the electron affinity and ionization potential, ε_L and ε_H are the energies of the highest occupied molecular orbital (HOMO) and the lowest unoccupied molecular orbital (LUMO), respectively. Chemical hardness has been established as an electronic quantity that in many cases may be used to characterize the relative stability of molecules and aggregates through the principle of maximum hardness (PMH) proposed by Pearson [30]. The PMH asserts that molecular systems at equilibrium present the highest value of hardness. The hardness of Al_nAs clusters, calculated according to Eq. (5) using VIP for the ionization potential and VEA for the electron affinity, is shown in Fig. 7. Assuming that the PMH holds in these systems, we expect the hardness to present an oscillating behavior with local maxima at the clusters with even valence-electron clusters, as found for the VEA, and the relative energy in Figs. 3 and 6 shows that the even valence-electron clusters present higher values of hardness than their neighboring clusters. We observe the even-odd oscillating feature similar to that already stressed in the VEA, and stability criteria. Stable clusters are harder than their neighbors' odd valence-electron systems.

We present in Table 5 the static mean polarizability $\langle\alpha\rangle$ and mean polarizability per atom $(\langle\alpha\rangle/n+1)$ for the lowest-energy structures calculated within the B3LYP scheme. The static mean polarizability $\langle\alpha\rangle$ is calculated from the polarizability tensor components as

$$\langle\alpha\rangle = (\alpha_{XX} + \alpha_{YY} + \alpha_{ZZ}) \quad (6)$$

The static polarizability represents one of the most important observables for the understanding of the electronic properties of clusters, it is proportional to the number of electrons of the systems, and it is very sensitive to the delocalization of valence electrons as well as to the structure and shape of the system. In Table 5 we note that when going from Al_2As to $Al_{15}As$ the polarizability of the clusters increases monotonically showing the expected proportionality with n (or the total electrons number). We note in Table 5 that the mean polarizability per atom $(\langle\alpha\rangle/n+1)$ of Al_nAs clusters decreases from 49.3 a.u. for Al_2As to 37.0 a.u. for $Al_{15}As$, with the lowest value (37.0 a.u.) for $Al_{15}As$. The lowest value of polarizability per atom occurs for $Al_{15}As$, which can be due to a combined effect of the compactness of structure and the electronic shell closure that occurs for this cluster. The closed-shell electronic configuration of $Al_{15}As$ will result in the low response of the electrons to the applied electric field, resulting, thereby, in lower value of polarizability. Chattaraj et al. have proposed a minimum polarizability principle (MPP) [31,32] which states that the natural direction of evolution of any system is toward a state of minimum polarizability. There are many studies confirming the validity of the MPP on different kind of reactions and systems. So we can speculate the $Al_{15}As$ cluster is a stable cluster. It is also evident from Table 5 that the odd–even oscillations, which are present in the dissociation energy, the second-order energy differences, VEA and hardness, are not seen here.

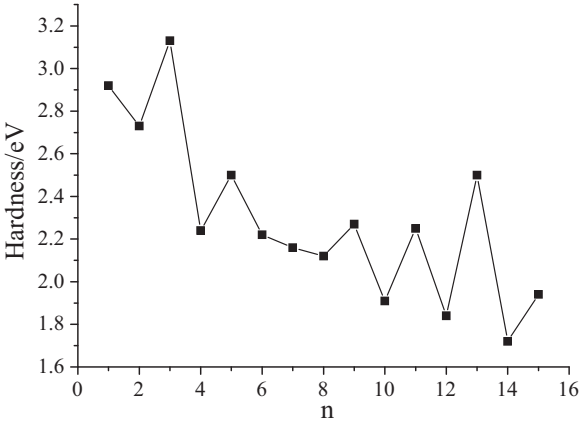

Fig. 7. Hardness of Al_nAs cluster.

4. Summary and conclusions

Aluminum clusters doped with a single As impurity atom has been studied by an all-electron linear combination of atomic orbital approach, within spin-polarized density functional theory, using the GGA scheme for the exchange-correlation. The As impurity is found to occupy a peripheral position. The stability of the lowest-energy structures is investigated by analyzing energies. Odd–even oscillations are observed in most of the physical properties investigated, suggesting that clusters with an even number of electrons are more stable than their odd-electron neighboring clusters.

Acknowledgments

This work is financially supported by the National Natural Science Foundation of China (Grant No. 20603021), Youth Foundation of Shanxi (Grant No. 2007021009) and the Youth Academic Leader of Shanxi.

References

[1] B.K. Rao, P. Jena, J. Chem. Phys. 111 (1999) 1890.
[2] M.D. Deshpande, D.G. Kanhere, I. Vasiliev, R.M. Martin, Phys. Rev. B 68 (2003) 035428.
[3] G.W. Turner, R.L. Johnston, N.T. Wilso, J. Chem. Phys. 112 (2000) 4773.
[4] J. Akola, M. Manninen, H. Hakkinen, U. Landman, X. Li, L.S. Wang, Phys. Rev. B 62 (2000) 13216.
[5] U. Rothlisberger, W. Andreoni, J. Chem. Phys. 94 (1992) 8129.
[6] Z.Y. Liu, C.R. Wang, R.B. Huang, L.S. Zheng, Int. J. Mass Spectrom. 141 (1995) 201.
[7] W. Andreoni, Phys. Rev. B. 45 (1992) 4203.
[8] H.K. Quek, Y.P. Feng, C.K. Ong, Z. Phys. D 42 (1997) 309.
[9] V. Tozzini, F. Buda, A. Fasolino, J. Phys. Chem. B 105 (2001) 12477.
[10] A. Costales, A.K. Kandalam, R. Franco, R. Pandey, J. Phys. Chem. B 106 (2002) 1940.
[11] E.F. Archibong, A. St-Amant, J. Phys. Chem. A 106 (2002) 7390.
[12] P.Y. Feng, D. Dai, K. Balasubramanian, J. Phys. Chem. A 104 (2000) 422.
[13] X. Zhu, J. Mol. Struct. (Theochem) 638 (2003) 99.

[14] R.G. Parr, W. Yang, Density Functional Theory of Atoms and Molecules, Oxford University Press, New York, 1989.
[15] R.O. Jones, O. Gunnarsson, Rev. Mod. Phys. 61 (1989) 689.
[16] (a) M.M. Francl, W.J. Petro, W.J. Hehre, J.S. Binkley, M.S. Gordon, D.J. DeFrees, J.A. Pole, J. Chem. Phys. 77 (1982) 3654;
(b) P.C. Hariharan, J.A. Pople, Theor. Chim. Acta 28 (1973) 213.
[17] S.H. Vosko, L. Wilk, M. Nusair, Can. J. Phys. 58 (1980) 1200.
[18] D. Ceperley, M.B. Alder, J. Phys. Rev. Lett. 45 (1980) 566.
[19] M.J. Frisch, G.W. Trucks, H.B. Schlegel, G.E. Scuseria, M.A. Robb, J.R. Cheeseman, J.A. Montgomery, Jr., T. Vreven, K.N. Kudin, J.C. Burant, J.M. Millam, S.S. Iyengar, J. Tomasi, V. Barone, B. Mennucci, M. Cossi, G. Scalmani, N. Rega, G.A. Petersson, H. Nakatsuji, M. Hada, M. Ehara, K. Toyota, R. Fukuda, J. Hasegawa, M. Ishida, T. Nakajima, Y. Honda, O. Kitao, H. Nakai, M. Klene, X. Li, J.E. Knox, H.P. Hratchian, J.B. Cross, V. Bakken, C. Adamo, J. Jaramillo, R. Gomperts, R.E. Stratmann, O. Yazyev, A.J. Austin, R. Cammi, C. Pomelli, J.W. Ochterski, P.Y. Ayala, K. Morokuma, G.A. Voth, P. Salvador, J.J. Dannenberg, V.G. Zakrzewski, S. Dapprich, A.D. Daniels, M.C. Strain, O. Farkas, D.K. Malick, A.D. Rabuck, K. Raghavachari, J.B. Foresman, J.V. Ortiz, Q. Cui, A.G. Baboul, S. Clifford, J. Cioslowski, B.B. Stefanov, G. Liu, A. Liashenko, P. Piskorz, I. Komaromi, R.L. Martin, D.J. Fox, T. Keith, M.A. Al-Laham, C.Y. Peng, A. Nanayakkara, M. Challacombe, P.M.W. Gill, B. Johnson, W. Chen, M.W. Wong, C. Gonzalez, J.A. Pople, computer code Gaussian 03; Gaussian, Inc., Wallingford, CT, 2004.
[20] A.D. Becke, Phys. Rev. A 38 (1988) 3098.
[21] C. Lee, W. Yang, R.G. Parr, Phys. Rev. B 37 (1988) 785.
[22] X. Chi, S. Tian, K. Xu, Chin. J. Chem. Phys. 15 (2002) 22.
[23] K.P. Huber, G. Herzberg, Molecular Spectra and Molecular Structure. I. Constants of Diatomic Molecules, Van Nostrand Reinhold, New York, 1979.
[24] S.N. Khanna, P. Jena, Phys. Rev. Lett. 69 (1992) 1664.
[25] X.S. Zhu, J. Mol. Struct. (Theochem) 638 (2003) 99.
[26] J. Xiang, S.H. Wei, X.H. Yan, J.Q. You, Y.L. Mao, J. Chem. Phys. 120 (2004) 4251.
[27] G. Zhao, J. Zhang, Q. Jing, Y. Luo, Y. Wang, J. Chem. Phys. 127 (2007) 234312.
[28] B.L. Wang, J.J. Zhao, D.N. Shi, X.S. Chen, G.H. Wang, Phys. Rev. A 72 (2005) 023204.
[29] R.G. Parr, R.G. Pearson, J. Am. Chem. Soc. 105 (1983) 7512.
[30] R.G. Pearson, Chemical Hardness Applications from Molecules to Solids, Wiley-VCH, Weinheim, 1997.
[31] P.K. Chattaraj, S. Sengupta, J. Phys. Chem. 100 (1996) 16126.
[32] P.K. Chattaraj, P. Fuentealba, P. Jaque, A. Toro-Labbe, J. Phys. Chem. A 103 (1999) 9307.